

# Uniaxial Strain Induced Topological Phase Transition in Bismuth-Tellurohalide–Graphene Heterostructures

Zoltán Tajkov, János Koltai\*, Dávid Visontai, László Oroszlány

Zoltán Tajkov, János Koltai, *Department of Biological Physics, ELTE Eötvös Loránd University, Pázmány P. s. 1/A, H-1117, Budapest, Hungary*

Dávid Visontai, *Department of Materials Physics, ELTE Eötvös Loránd University, Pázmány P. s. 1/A, H-1117, Budapest, Hungary*

László Oroszlány, *Department of Physics of Complex Systems, ELTE Eötvös Loránd University, Pázmány P. s. 1/A, H-1117, Budapest, Hungary and MTA-BME Lendület Topology and Correlation Research Group, Budapest University of Technology and Economics, Budafoki út 8., H-1111 Budapest, Hungary*

## 1 Abstract

We explore the electronic structure and topological phase diagram of hybrid systems formed of graphene and ternary bismuth tellurohalide layers. We show that mechanical stress inherently present in fabricated samples could easily induce a topological phase transition in single-sided heterostructures, turning the sample into a novel experimental realization of a time reversal invariant topological insulator. We construct an effective tight-binding description for low energy excitations and fit model parameters to *ab initio* band structures. We propose a simple approach for predicting phase boundaries as a function of mechanical distortions and hence gain a deeper understanding on how the topological phase in the considered system may be engineered.

## 2 Introduction

In quantum confined nanostructures the electron-spin dephasing time can reach the order of microseconds,<sup>[1–3]</sup> providing an exceptional venue for information processing and information transmission, such as spin-based devices for conventional computers or quantum computing.<sup>[4–7]</sup> A key difference between spintronic devices and conventional electronics is the controllable manipulation of the spin degree of freedom of charge carriers. Manipulating spins without an external magnetic field is necessary for several technological applications.<sup>[8]</sup> Strong spin-orbit coupling (SOC) in layered two dimensional (2D) structures potentially leads to band inversion driving the system through a topological phase transition.<sup>[9–11]</sup> The thus created novel quantum phase hosts topologically protected edge states whose spin is locked to their propagation direction.<sup>[12]</sup> These spin-momentum locked robust edge states allow for manipulation of the electron spin, hence they have potential as architectural components in a future quantum information processing device.<sup>[13–16]</sup>

Since its first isolation graphene emerged as an ideal template material for revolutionary applications.<sup>[17]</sup> Although graphene proved to be an excellent electronic conductor with outstanding mechanical properties, the SOC is inherently weak in it due to the small atomic weight of carbon atoms.<sup>[18,19]</sup> Several theoretical proposals have been made to overcome this limitation for example with introducing curvature or by means of adatoms.<sup>[20,21]</sup> From an engineering point of view hybrid

---

\*Corresponding author e-mail address: Janos Koltai <koltai@elte.hu>

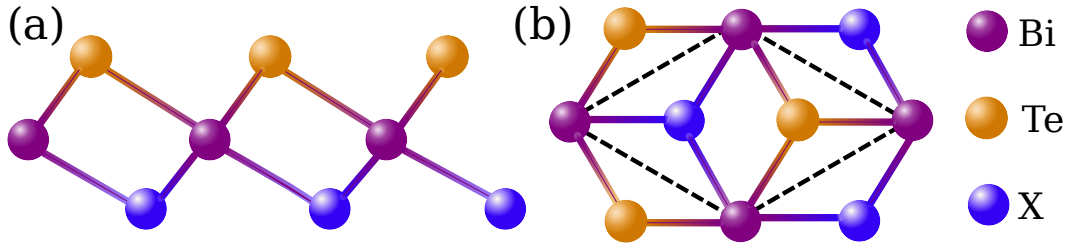


Figure 1: Side (a) and top (b) view of the structure of a monolayer of the BiTeX (X = I, Br, Cl) crystal. The black dashed line indicates the unit cell.

2D heterostructures, due to already existing and well understood fabrication procedures, seem a more practical approach for introducing a host of exotic features in graphene samples.<sup>[22]</sup> Thus this method has the potential to introduce a considerably large SOC in graphene based devices utilizing layered materials with a strong spin-orbit interaction.

Ternary bismuth tellurohalides are a new class of polar crystals with a layered structure represented by BiTeX (X = I, Br, Cl).<sup>[23]</sup> The key constituent of these compounds is Bi, which is a heavy element and has a strong atomic SOC. Its triangular lattice layer is stacked between a Te and a halogen atom layer, see **Figure 1**. The already large intrinsic SOC in Bi and the structural asymmetry combined with a large in-plane gradient of the crystal field in this lattice results in giant Rashba spin-splitting semiconductors.<sup>[24–28]</sup> Among these BiTeI stands out with the strongest SOC.<sup>[29]</sup> Recently the first experimental isolation and characterization of a single layer of BiTeI was reported by Fülöp *et al.* using a novel exfoliation technique.<sup>[30]</sup> It was also shown that albeit the band gap increased, the basic characteristics of bulk BiTeI is preserved, hence this material can be used as a strong SOC inducing component in graphene based heterostructures as it was theoretically studied in previous works.<sup>[31,32]</sup>

In this manuscript, we give an account of a detailed theoretical investigation of heterostructures consisting of graphene and BiTeX layered van der Waals systems. Based on first principle calculations we distilled an effective model in order to understand the emerging topological phase in the studied structures and explored the phase diagram of the system as a function of mechanical distortions. We identify single-sided BiTeX-graphene heterostructures as promising candidates for engineering mechanically controllable topological phases.

## 3 First principles results

### 3.1 Electronic structure of BiTeX-graphene hybrid systems

The crystal structure of BiTeX is characterized by similar experimental in-plane lattice constants  $a_{\text{BiTeX}} = 4.34 \text{ \AA}$ ,  $4.24 \text{ \AA}$ ,  $4.27 \text{ \AA}$  for (X = I, Br, Cl) respectively.<sup>[33]</sup> As these values are approximately  $\sqrt{3}$  times bigger than the lattice constant of graphene ( $a_C = 2.46 \text{ \AA}$ ), it is possible to find a commensurate supercell by the  $30^\circ$  rotation of the graphene layer. This supercell is depicted in **Figure 2(a)** consisting of six carbon atoms, one bismuth, one tellurium and one halogen atom. Note that this choice leads to a strain not larger than 1.8% in the BiTeX lattice. Furthermore we only consider the so called hollow configuration, that is when the adjacent atom

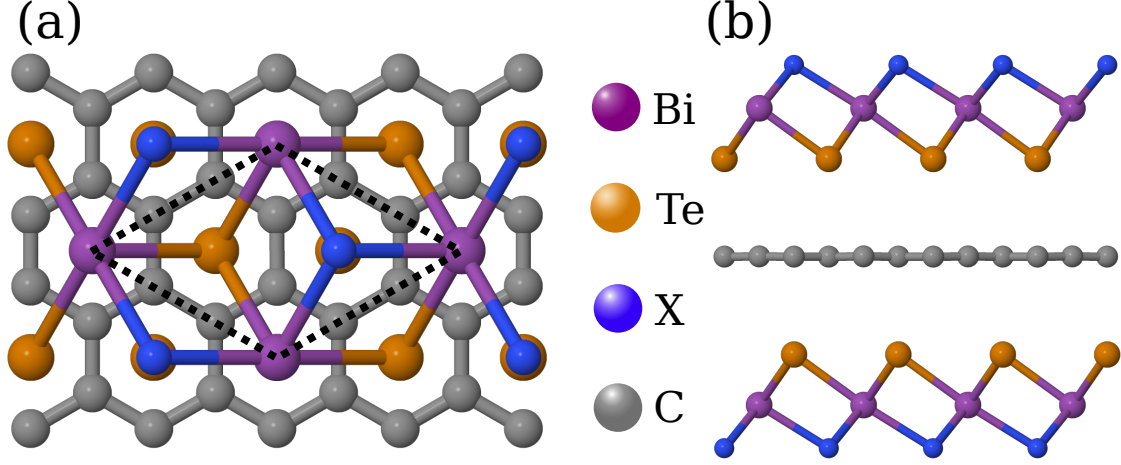


Figure 2: Top (a) and side (b) view of the structure of graphene/BiTeX ( $X = \text{I, Br, Cl}$ ) sandwich. The black dashed line indicates the unit cell.

Structure	$d$ [Å]	$E_{gap}$ [meV]	$\mathbb{Z}_2$
BiTeI - C	3.44	$\approx 1$	trivial
$2 \times \text{BiTeI} - \text{C}$	3.42	metallic	N.A.
BiTeI - C [I faced]	3.35	metallic	N.A.
BiTeI - C - BiTeI	3.45	44	topological
BiTeI - C - $2 \times \text{BiTeI}$	3.46	metallic	N.A.
$2 \times \text{BiTeI} - \text{C} - 2 \times \text{BiTeI}$	3.44	metallic	N.A.
BiTeCl - C	3.46	$\approx 1$	trivial
$2 \times \text{BiTeCl} - \text{C}$	3.44	metallic	N.A.
BiTeCl - C [Cl faced]	3.00	metallic	N.A.
BiTeCl - C - BiTeCl	3.46	41	topological
BiTeCl - C - $2 \times \text{BiTeCl}$	3.44	metallic	N.A.
$2 \times \text{BiTeCl} - \text{C} - 2 \times \text{BiTeCl}$	3.53	metallic	N.A.
BiTeBr - C	3.44	$\approx 1$	trivial
$2 \times \text{BiTeBr} - \text{C}$	3.39	metallic	N.A.
BiTeBr - C [Br faced]	3.09	metallic	N.A.
BiTeBr - C - BiTeBr	3.46	42	topological
BiTeBr - C - $2 \times \text{BiTeBr}$	3.45	metallic	N.A.
$2 \times \text{BiTeBr} - \text{C} - 2 \times \text{BiTeBr}$	3.44	metallic	N.A.
BiTeI - C - BiTeCl	3.44	42	topological
BiTeI - C - BiTeBr	3.47	44	topological
BiTeBr - C - BiTeCl	3.44	43	topological

Table 1: Table of the considered structures. First column denotes the geometry, where C indicates the graphene layer. The Te layers of BiTeX face graphene, unless indicated otherwise. Second and third columns are the layer distance between graphene and BiTeX, and the band gap calculated by SIESTA, where "metallic" keyword signifies the absence of a direct band gap. The fourth column is the value of the  $\mathbb{Z}_2$  invariant for insulating systems.

of the BiTeX layer (*i.e.*, Te or X) is positioned above the center of a hexagon of carbon atoms in the graphene layer, as it was shown previously that this horizontal configuration is the most stable.<sup>[31]</sup>

We compared various combinations of the two constituents of the investigated heterostructure, BiTeX layers and graphene. First we studied single-sided setups, comprising of a single layer of graphene and one or two layers of BiTeX, taking both Te and X faced alignments into account. We also dealt with two sided "sandwich" structures, where the graphene sheet is surrounded by one or two layers of BiTeX from both sides. In the investigated sandwich structures Te layers were always facing graphene. The initial geometry of all considered configurations were fully relaxed, allowing also for change of the in-plane lattice parameter. We found however that in all cases the optimal geometry yielded the in-plane lattice constant of graphene, as expected due to the larger stiffness of graphene.<sup>[34]</sup> The obtained optimal layer distances, bulk band gap of electronic states (if any) and topological  $\mathbb{Z}_2$  invariant (for insulators) are compiled in **Table 1**.

The layer distance between BiTeX and graphene was found to be around 3.4 Å for all considered arrangements, thus one can safely conclude that the inter-layer interaction in these systems is of van der Waals type. For the single-sided Br or Cl faced BiTeX graphene configurations the interlayer distance was found significantly reduced compared to other cases. This tendency correlates well to the widely accepted, experimentally extracted van der Waals radii, which are also definitely lower for Br and Cl atoms compared to Te and I atoms.<sup>[35,36]</sup>

In **Figure 3** we present the calculated electronic band structures for all considered BiTeBr-graphene structures around the Fermi energy. Coloring of the bands corresponds to the orbital weights of the constituent layers, carbon orbitals are shaded red while states localized to BiTeBr layers are depicted by blueish colors, a purple hue signifies a strongly hybridized state. Depending on the number of BiTeBr layers and their relative alignment the studied systems show several distinct features.

Figure 3 (a) and (b) depict single-sided and sandwich structures of Te faced monolayer BiTeBr-graphene arrangements for which cases the low energy spectrum is dominated by quasiparticle contributions localized to the carbon atoms, reminiscent of the Dirac cones of graphene. In these two cases the Dirac point is auspiciously tuned to the gap of the BiTeBr monolayer bands. Since these structures are primarily characterized by graphene like bands, they might be understood in terms of a simplified model where the  $p_z$  orbitals of carbon atoms are subject to an induced spin-orbit coupling (see section 4). The main difference between the single-sided and sandwich structures is that, while in the sandwich structure a sizable direct gap of 41 meV is present at the  $\Gamma$  point, in the single-sided system the calculation yields a considerably smaller gap of about 1 meV. We also extracted the  $\mathbb{Z}_2$  topological invariant by calculating the flow of Wannier centers in the half of the Brillouin zone<sup>[37,38]</sup> based on the *ab initio* Hamiltonian (for details see section 6). The topological classification of the sandwich structure confirms the findings of Kou and coworkers namely that the gap in sandwich structures is topological.<sup>[31]</sup> On the other hand based on our calculations the small gap in the single-sided system is trivial.

In the other investigated scenarios depicted in Figure 3 (c)-(f), in contrast to the Te faced monolayer BiTeBr-graphene arrangements, the image of the Dirac point is either considerably shifted away from the Fermi level or it is masked by states originating from BiTeBr, thus a strong mixing of BiTeBr and carbon bands

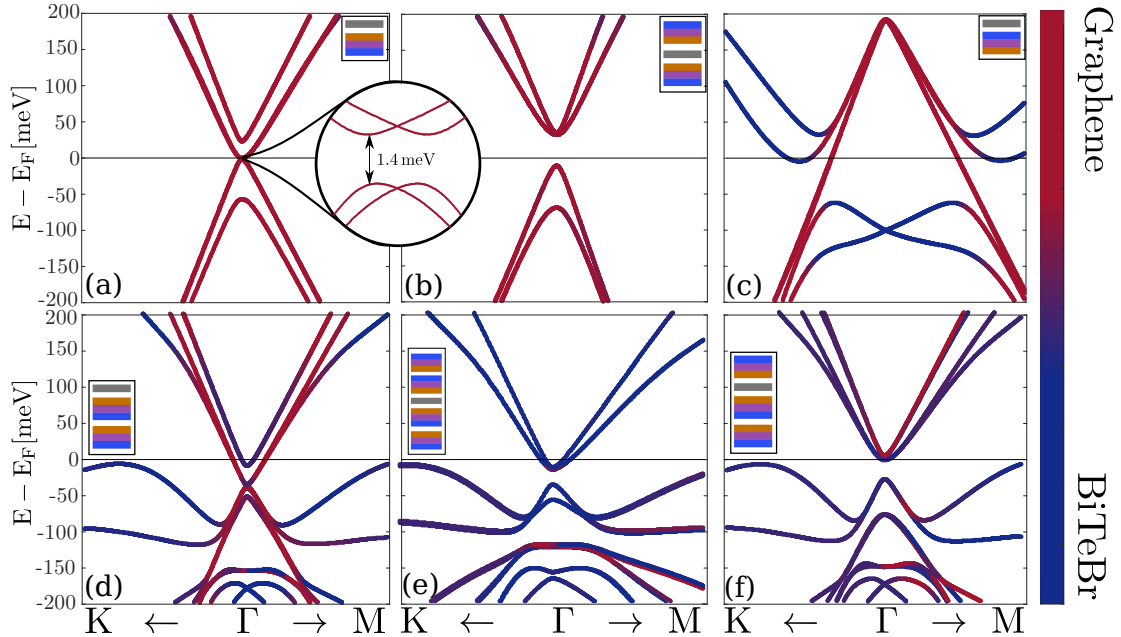


Figure 3: Electronic band structure of the considered geometries consisting of BiTeBr and graphene layers near the  $\Gamma$  point. Bands are colored based on the localization of the states they represent, hues of red indicate states localized to the graphene layer while blue denotes BiTeBr orbitals. Insets in all subfigures show the corresponding geometrical arrangement of atomic layers with the same color scheme as was introduced in Figure 2.

occurs, resulting in metallic band structures. Similar trends can be identified in other arrangements, independently from the type of halogen atom considered (cf. Table 1).

In the remainder of the manuscript we shall focus on the setups where the low energy electronic structure is dominated by the  $p_z$  orbitals of graphene. Therefore, we shall only consider the Te faced sandwich and the monolayer BiTeX-graphene arrangements.

### 3.2 Effects of mechanical distortions

Previously, we presented results obtained for relaxed geometries. Manufactured devices are commonly subject to mechanical distortions which in turn can have a non-negligible impact on the electronic properties of the system. Recently considerable experimental effort has been made to make use of strain fields to control electronic and optical properties of novel heterostructures.<sup>[39–42]</sup> Inspired by these advances, we investigate below how the electronic states and their topological character is influenced in Te faced single-sided BiTeBr-graphene heterostructure as the sample is subjected to in-plane uniaxial strain combined with stress perpendicular to the device.

We model in-plane uniaxial strain in our *ab initio* calculations by stretching the in-plane unit cell vectors along a carbon–carbon bond, and allowing the atomic positions relax in the constrained unit cell. On the other hand out-of-plane strain is simulated by reducing the distance between graphene and the BiTeX layer, without relaxation of the atomic positions.

We calculated the evolution of the size of the band gap and the topological

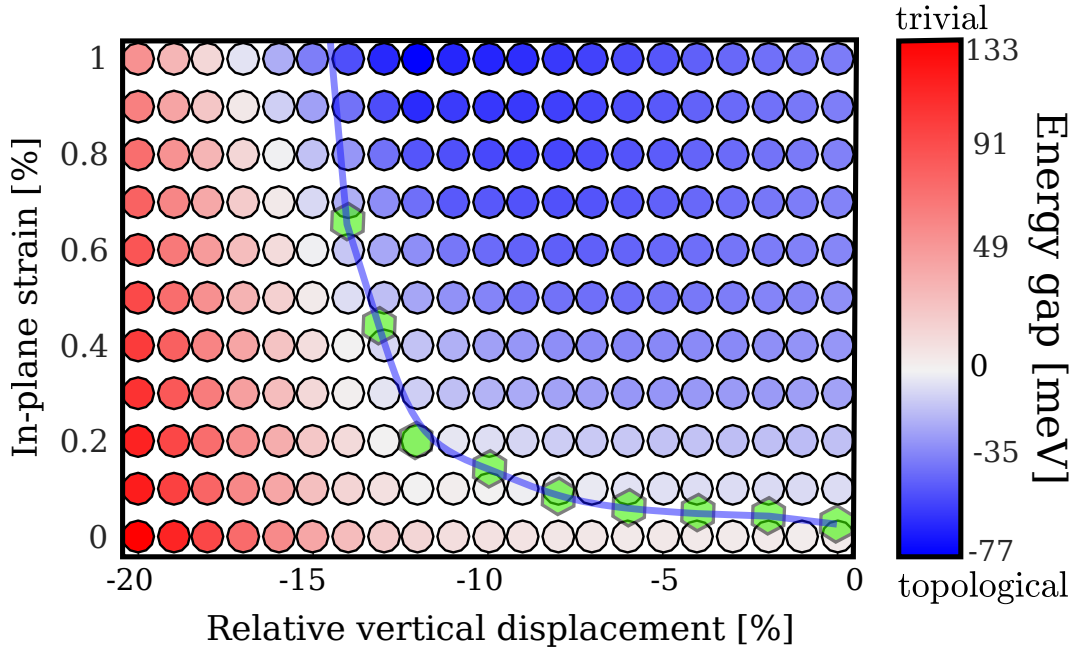


Figure 4: The circles show the *ab initio* phase diagram of the single-sided BiTeBr-graphene heterostructure in the presence of mechanical distortion. Topological band gaps are denoted by negative values. Green hexagons (connected with a blue tentative curve) trace out the tight binding phase boundary (see text for more details).

index as both in-plane and out-of-plane strain was varied. The corresponding phase diagram is shown on **Figure 4**. The sign of the band gap indicates the topological invariant, it is negative if the system is topological, positive otherwise.

Based on the presented results we conclude that both type of mechanical distortions have a striking effect on the band gap, however they favor different topological phases. Out-of-plane strain widens the initially present trivial band gap, while in-plane strain drives the system in the topological phase. We only present results for BiTeBr further calculations show that BiTeCl behaves qualitatively in the same fashion. BiTeI turns metallic instead of a trivial insulator due to some non-graphene bands reaching the Fermi level as pressure is increased.

We note that the largest out-of-plane strain we applied would correspond to a nominal pressure of 20 GPa, which we estimated as the energy derivation per unit area over the reduced distance. The mechanical stresses considered in our calculations can thus be routinely achieved in current day experimental setups.<sup>[43–47]</sup>

## 4 Low energy description

### 4.1 A model Hamiltonian

In the previous section, based on first principles calculations, we identified two arrangements from all the considered structures where electronic states close to the Fermi energy are dominated by the  $p_z$  orbitals of carbon atoms. These two setups, the Te faced single-sided BiTeX-graphene heterostructure and the sandwich system, are depicted in the insets of Figure 3 (a) and (b). In this section we propose an effective model, based on the tight binding (TB) description of graphene, where due

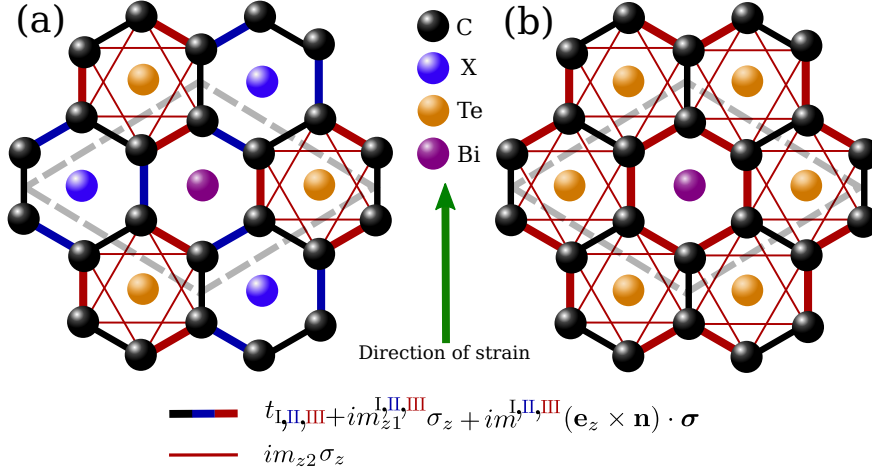


Figure 5: Illustration of the tight binding model of the graphene/BiTeX heterostructures for single-sided (a) and sandwich (b) arrangements.

to the presence of BiTeX layers an appropriately patterned SOC emerges. With the help of the introduced model we gain a deeper insight into the mechanisms responsible for the emergence of the topological phase witnessed before. Our effective description of the heterostructure is cast in a form that is digestible for theoretical approaches calculating electron, thermal and spin transport properties of samples on experimentally relevant scales.<sup>[48,49]</sup>

Respecting the symmetries of the system studied in the first principles calculations, we introduce a model with only a minimal number of parameters. Beyond the usual hopping integrals  $t$ , we assume spin-orbit interaction compatible with time reversal symmetry on nearest neighbor carbon-carbon bonds as  $i\mathbf{m}\boldsymbol{\sigma}$ , where  $\mathbf{m}$  is a real vector,  $\boldsymbol{\sigma}$  is the vector of Pauli matrices. We also include second nearest neighbor out-of-plane spin-orbit interaction as it was previously proposed by Kane and Mele to germinate a topological phase transition in graphene like systems.<sup>[50]</sup> The studied systems are invariant under  $C_{3v}$  rotations of the plane. The in-plane component of the  $\mathbf{m}$  vector on each bond is restricted by this symmetry and points perpendicular to the bonds<sup>[51]</sup>. After taking into account all the symmetries of the system our simplified model is depicted on **Figure 5**. We thus introduce three different nearest neighbor hopping integrals  $t_{I,II,III}$ , three in-plane  $m^{I,II,III}$  and three out-of-plane  $m_{z1}^{I,II,III}$  spin-orbit interaction magnitudes and a second-nearest neighbor out-of-plane spin-orbit interaction strength  $m_{z2}$ .

In the absence of the BiTeX layers graphene also possesses inversion symmetry with an inversion center in the middle of each hexagon. This symmetry is altered in the case of the sandwich arrangement in such a way that only hexagon centers aligned with Bi atoms remain inversion centers. In this case inversion symmetry forbids SOC on first nearest-neighbor bonds (denoted by thick black lines in Figure 5b), while it connects the hopping and SOC magnitudes along bonds marked by red and blue lines. That is  $t_{II} = t_{III}$ ,  $m^{II} = m^{III} = m$  and  $m_{z1}^{II} = m_{z1}^{III} = m_{z1}$  while  $m^I = m_{z1}^I = 0$ . We now make some further assumptions regarding the actual investigated system. Since the interaction between BiTeX and graphene is van der Waals type and the Bi atoms are further away from the graphene sheet as the Te atoms we neglect the second nearest neighbor SOC on the hexagonal plaquettes encircling Bi atoms.

Breaking inversion symmetry by separating one of the BiTeX layer from

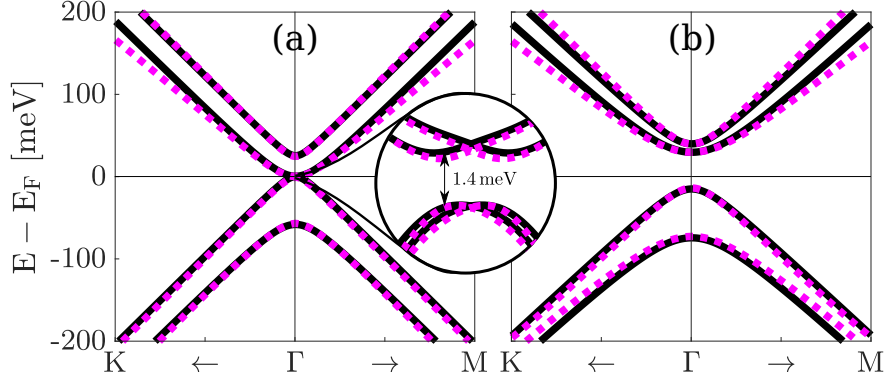


Figure 6: The band structure of the single-sided (a) and the sandwich (b) BiTeBr-graphene heterostructure in the low energy range near the  $\Gamma$ -point. Solid black lines indicate the first principles result and dotted magenta lines mark our fitted tight binding bands. For the fitted parameters see **Table 2**.

the sandwich structure results in a Te faced single-sided geometry. In this case nearest neighbor SOC is allowed on thick black bonds, and blue and red bonds are no longer connected. Consistently with our previous approach we neglect second nearest neighbor SOC on the plaquettes encircling X atoms since they are even further from the graphene sheet as Bi. Therefore the single-sided setup is characterized by 10 different parameters, the hopping amplitudes  $t_i$ , first nearest neighbor in-plane SOC  $m^i$  and out-of plane SOC  $m_{z1}^i$  with  $i = \text{I, II, III}$  and the only second nearest neighbor SOC  $m_{z2}$  in hexagons surrounding Te atoms.

We thus constructed the Hamiltonian as:

$$\begin{aligned}
H = \sum_{\alpha} \sum_{\substack{p=1,3,5 \\ q=2,4,6}} \left[ \left( t_{\text{II}} \sigma_0 + im_{z1}^{\text{II}} \sigma_z + im^{\text{II}} (\mathbf{e}_z \times \mathbf{n}_{\alpha\alpha pp+1}) \cdot \boldsymbol{\sigma} \right) \hat{c}_{\alpha p}^{\dagger} \hat{c}_{\alpha p+1} \right. \\
\left. + \left( t_{\text{III}} \sigma_0 + im_{z1}^{\text{III}} \sigma_z + im^{\text{III}} (\mathbf{e}_z \times \mathbf{n}_{\alpha\alpha qq+1}) \cdot \boldsymbol{\sigma} \right) \hat{c}_{\alpha q}^{\dagger} \hat{c}_{\alpha q+1} \right] \\
+ \sum_{\substack{\langle \alpha\gamma \rangle \\ \langle pq \rangle}} \left( t_{\text{I}} \sigma_0 + im_{z1}^{\text{I}} \sigma_z + im^{\text{I}} (\mathbf{e}_z \times \mathbf{n}_{\alpha\gamma pq}) \cdot \boldsymbol{\sigma} \right) \hat{c}_{\alpha p}^{\dagger} \hat{c}_{\gamma q} \\
+ \sum_{\substack{\langle \alpha\gamma \rangle \\ \langle\langle pq \rangle\rangle}} im_{z2} \sigma_z \hat{c}_{\alpha p}^{\dagger} \hat{c}_{\gamma q} + h.c..
\end{aligned} \tag{1}$$

The sum in  $\alpha$  and  $\gamma$  goes over all unit cells in the crystal, while  $p, q$  indicate one of the six atoms in a given unit cell. Annihilation (creation) operators for an electron in unit cell  $\alpha$  on site  $p$  are denoted by  $\hat{c}_{\alpha p}^{(\dagger)}$ ,  $\mathbf{e}_z$  is a unit vector pointing in the  $z$  direction,  $\mathbf{n}_{\alpha\gamma pq}$  is the vector that points from site  $i$  in unit cell  $\alpha$  to site  $j$  in unit cell  $\gamma$  and  $\sigma_0$  is the  $2 \times 2$  identity operator.

The fitted and first principles band structure are depicted together for both the single-sided and sandwich structures in **Figure 6**. In the following we map the topological character of the introduced two models. Tracking again the evolution of Wannier centers yields the  $\mathbb{Z}_2$  topological invariant for the proposed effective Hamiltonian.<sup>[37,38]</sup> First we investigate the inversion symmetric sandwich setup, and focus on the parameters responsible for spin-orbit interaction,  $m$ ,  $m_{z1}$  and  $m_{z2}$  while fixing the two hopping terms to  $t_{\text{I}} = 2.227$  eV and  $t_{\text{II}} = 2.210$  eV. The phase diagram in **Figure 7** shows two topologically distinct insulating phases and a metallic phase. We observe that without SOC but in the presence of a hopping

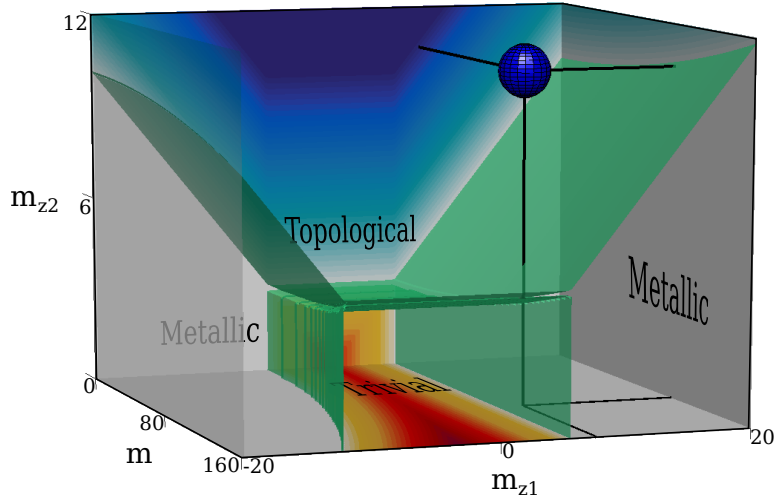


Figure 7: Topological phase diagram of the inversion symmetric graphene/BiTeBr structure described by **Equation 1** in the case of  $t_I = 2.227$  eV and  $t_{II} = 2.210$  eV. The  $m$ ,  $m_{z1}$  and  $m_{z2}$  parameters are shown in units of meV.

mismatch the model is a trivial Kekulé patterned band insulator as it was studied in clean graphene under appropriate biaxial strain.<sup>[52]</sup> The first nearest neighbor out-of plane SOC  $m_{z1}$  drives the system towards a gapless metallic phase, while the second nearest neighbor SOC  $m_{z2}$  promotes the topological insulator phase, large  $m$  eventually makes a trivial insulator as it also does in more simple models.<sup>[50]</sup> A blue sphere denotes the parameter configuration that represent the fit to the *ab initio* result for the sandwich configuration.

Structure	$t_I$	$t_{II}$	$t_{III}$	$m^I$	$m^{II}$	$m^{III}$	$m_{z1}^I$	$m_{z1}^{II}$	$m_{z1}^{III}$	$m_{z2}$
BiTeI - C	2375	2324	2346	-19.45	-421.0	-426.5	-5.917	4.822	40.50	-6.873
BiTeBr - C	2355	2323	2338	-1.964	-433.6	-434.2	0.910	0.513	29.18	-8.376
BiTeCl - C	2365	2350	2370	-7.472	-40.60	-40.00	-4.347	-16.04	21.55	-11.61
BiTeI - C - BiTeI	2268	2274		0	146.9		0	-7.304		11.15
BiTeBr - C - BiTeBr	2227	2210		0	138.4		0	-11.90		10.64
BiTeCl - C - BiTeCl	2251	2258		0	129.8		0	-6.040		9.900

Table 2: Table of the fitted tight binding parameters (meV) as defined in the Hamiltonian Equation 1

## 4.2 Understanding the role of mechanical distortions

Turning our attention to the single-sided arrangements our main goal is to understand the phase diagram emerging from the first principles calculations presented in Figure 4 describing a topological phase transition driven by in-plane uniaxial strain and pressure perpendicular to the sample. In the absence of in-plane distortions but under out-of-plane strain the system can still be well approximated by the model described in the previous section. Unavoidably, the application of uniaxial deformation breaks  $C_{3v}$  symmetry of the system. We included this effect into our model by multiplying all first nearest neighbor hopping and SOC terms in the direction of the uniaxial strain by a common factor  $e^{-\beta(l/l_0-1)}$ .<sup>[53]</sup> In this multiplicative term  $l_0$  is the bond length in stress free system,  $l$  is the bond length in the deformed case and  $\beta = 2.384$  is a dimensionless parameter determined from fitting to *ab initio* cal-

culations performed on freestanding graphene. This approach is widely used in the literature for describing the effects of mechanical distortions on TB parameters.<sup>[53,54]</sup> We note that following common practice bonds not parallel with the distortion were not modified. We also remark that this method is applicable for small to moderate strain values where buckling of the hexagons is negligible.<sup>[55]</sup>

Using this simple model for in-plane distortions we are now equipped for exploring the phase diagram of the effective system. We first fit our  $C_{3v}$  symmetric model to *ab initio* calculations performed for geometries without uniaxial in-plane strain. Introducing strain in these models as described above we calculate the size of the quasi particle gap and the topological invariant. The obtained results, depicted with green hexagons in Figure 4, show that for all cases the initially present trivial gap closes and a topological gap opens as one tunes the multiplicative factor representing the uniaxial strain. As it can be observed in Figure 4. our rudimentary approach for including the strain in the effective model adequately predicts the boundary of the topological phase, even for moderately large pressures, thus justifying its application.

## 5 Conclusion

In summary, we explored the rich topological phase diagram of bismuth tellurohalide/graphene heterostructures by means of first principles calculations. Based on our *ab initio* results we distilled a simple tight binding description for the investigated system capturing all relevant features of the low energy spectra of quasiparticles. We have demonstrated that the topological phase transition due to mechanical distortions in one-sided systems leads to a novel realization of the time reversal invariant topological insulating phase, thus making these heterostructures potential candidates for quantum technology applications.

## 6 Methods

The optimized geometry and ground state Hamiltonian and overlap matrix elements of each structure were self consistently obtained by the SIESTA implementation of density functional theory (DFT)<sup>[56,57]</sup>. SIESTA employs norm-conserving pseudopotentials to account for the core electrons and linear combination of atomic orbitals to construct the valence states. For all cases the considered samples were separated with a minimum of 18.5 Å thick vacuum in the perpendicular direction. The generalized gradient approximation of the exchange and the correlation functional was used with Perdew-Burke-Ernzerhof parametrization<sup>[58]</sup> and the pseudopotentials optimized by Rivero *et al.*<sup>[59]</sup> with a double- $\zeta$  polarized basis set and a real-space grid defined with an equivalent energy cutoff of 1000 Ry. The Brillouin zone integration was sampled by a  $24 \times 24 \times 1$  Monkhorst-Pack  $k$ -grid.<sup>[60]</sup> The geometry optimizations were performed until the forces were smaller than 10 meV/Å. The choice of pseudopotentials optimized by Rivero *et al.* ensures that both the obtained geometrical structures and the electronic band properties are reliable. As a benchmark we validated our method by comparing properties of the bulk graphite and bulk BiTeI with the experimental data.<sup>[29,61]</sup>

The fitting procedure was carried out by applying a constrained least squares minimization procedure to the difference between the TB and the DFT band energies. As one progresses further in energy away from the Fermi level the

assumption that carbon  $p_z$  orbital contributions dominate begins to break down, with significant BiTeX orbital contributions at energies around  $\pm 300$  meV. Therefore we fit the model to only 8 bands in an energy window of  $\pm 200$  meV. The fit is carried out over 720 points in  $\mathbf{k}$ -space along the high symmetry lines of the Brillouin zone.

## 7 Acknowledgement

This work was financially supported by the the Hungarian National Research, Development and Innovation Office (NKFIH) via the National Quantum Technologies Program 2017-1.2.1-NKP-2017-00001; grants no. K112918, K115608, FK124723 and K115575. This work was completed in the ELTE Excellence Program (1783-3/2018/FEKUTSRAT) supported by the Hungarian Ministry of Human Capacities. LO, JK acknowledge the Bolyai and Bolyai+ program of the Hungarian Academy of Sciences. We acknowledge [NIIF] for awarding us access to resource based in Hungary at Debrecen.

## References

- [1] D. D. Awschalom and J. M. Kikkawa, *Physics Today* **52**(6), 33–38 (1999).
- [2] J. R. Petta, A. C. Johnson, J. M. Taylor, E. A. Laird, A. Yacoby, M. D. Lukin, C. M. Marcus, M. P. Hanson, and A. C. Gossard, *Science* **309**(5744), 2180–2184 (2005).
- [3] R. Hanson, L. P. Kouwenhoven, J. R. Petta, S. Tarucha, and L. M. K. Vandersypen, *Reviews of Modern Physics* **79**(4), 1217–1265 (2007).
- [4] G. Burkard, H. A. Engel, and D. Loss, *Fortschritte der Physik* **48**(9), 965–986 (2000).
- [5] M. N. Leuenberger and D. Loss, *Physica E: Low-dimensional Systems and Nanostructures* **10**(1-3), 452–457 (2001).
- [6] J. M. Clemente-Juan, E. Coronado, and A. Gaita-Ariño, *Chemical Society Reviews* **41**(22), 7464–7478 (2012).
- [7] S. V. Eremeev, S. S. Tsirkin, I. A. Nechaev, P. M. Echenique, and E. V. Chulkov, *Scientific Reports* **5**(1), 12819 (2015).
- [8] I. Žutić, J. Fabian, and S. Das Sarma, *Reviews of Modern Physics* **76**(2), 323–410 (2004).
- [9] C. Niu, P. M. Buhl, G. Bihlmayer, D. Wortmann, S. Blügel, and Y. Mokrousov, *2D Materials* **3**(2), 025037 (2016).
- [10] Y. Ando and L. Fu, *Annual Review of Condensed Matter Physics* **6**(1), 361–381 (2015).
- [11] L. Fu, *Physical Review Letters* **106**(10), 106802 (2011).
- [12] M. Z. Hasan and C. L. Kane, *Reviews of Modern Physics* **82**(4), 3045–3067 (2010).

- [13] M. Freedman, A. Kitaev, M. Larsen, and Z. Wang, *Bulletin of the American Mathematical Society* **40**(1), 31–38 (2003).
- [14] A. Y. Kitaev, *Annals of Physics* **303**(1), 2–30 (2003).
- [15] C. Nayak, S. H. Simon, A. Stern, M. Freedman, and S. Das Sarma, *Reviews of Modern Physics* **80**(3), 1083–1159 (2008).
- [16] E. T. Campbell, B. M. Terhal, and C. Vuillot, *Nature* **549**(7671), 172–179 (2017).
- [17] K. S. Novoselov, A. K. Geim, S. V. Morozov, D. Jiang, Y. Zhang, S. V. Dubonos, I. V. Grigorieva, and A. A. Firsov, *Science* **306**(5696), 666–669 (2004).
- [18] N. Tombros, C. Jozsa, M. Popinciuc, H. T. Jonkman, and B. J. van Wees, *Nature* **448**(7153), 571–574 (2007).
- [19] A. H. Castro Neto and F. Guinea, *Physical Review Letters* **103**(2), 026804 (2009).
- [20] D. Huertas-Hernando, F. Guinea, and A. Brataas, *Physical Review B* **74**(15), 155426 (2006).
- [21] J. Balakrishnan, G. Kok Wai Koon, M. Jaiswal, A. H. Castro Neto, and B. Özyilmaz, *Nature Physics* **9**(5), 284–287 (2013).
- [22] A. K. Geim and I. V. Grigorieva, *Nature* **499**(7459), 419–425 (2013).
- [23] M. S. Bahramy, R. Arita, and N. Nagaosa, *Physical Review B* **84**(4) (2011).
- [24] C. R. Ast, J. Henk, A. Ernst, L. Moreschini, M. C. Falub, D. Pacilé, P. Bruno, K. Kern, and M. Grioni, *Physical Review Letters* **98**(18) (2007).
- [25] L. Wu, J. Yang, M. Chi, S. Wang, P. Wei, W. Zhang, L. Chen, and J. Yang, *Scientific Reports* **5**, 14319 (2015).
- [26] M. Sakano, J. Miyawaki, A. Chainani, Y. Takata, T. Sonobe, T. Shimojima, M. Oura, S. Shin, M. S. Bahramy, R. Arita, N. Nagaosa, H. Murakawa, Y. Kaneko, Y. Tokura, and K. Ishizaka, *Physical Review B* **86**(8) (2012).
- [27] C. J. Butler, H. H. Yang, J. Y. Hong, S. H. Hsu, R. Sankar, C. I. Lu, H. Y. Lu, K. H. O. Yang, H. W. Shiu, C. H. Chen, C. C. Kaun, G. J. Shu, F. C. Chou, and M. T. Lin, *Nature Communications* **5**(1), 4066 (2014).
- [28] Y. Qi, W. Shi, P. G. Naumov, N. Kumar, R. Sankar, W. Schnelle, C. Shekhar, F. C. Chou, C. Felser, B. Yan, and S. A. Medvedev, *Advanced Materials* **29**(18), 1605965 (2017).
- [29] K. Ishizaka, M. S. Bahramy, H. Murakawa, M. Sakano, T. Shimojima, T. Sonobe, K. Koizumi, S. Shin, H. Miyahara, A. Kimura, K. Miyamoto, T. Okuda, H. Namatame, M. Taniguchi, R. Arita, N. Nagaosa, K. Kobayashi, Y. Murakami, R. Kumai, Y. Kaneko, Y. Onose, and Y. Tokura, *Nat Mater* **10**(7), 521–526 (2011).

- [30] B. Fülöp, Z. Tajkov, J. Petó, P. Kun, J. Koltai, L. Oroszlány, E. Tóvári, H. Murakawa, Y. Tokura, S. Bordács, L. Tapasztó, and S. Csonka, *2D Materials* **5**(3), 031013 (2018).
- [31] L. Kou, S. C. Wu, C. Felser, T. Frauenheim, C. Chen, and B. Yan, *ACS Nano* **8**(10), 10448–10454 (2014).
- [32] Z. Tajkov, D. Visontai, P. Rakyta, L. Oroszlány, and J. Koltai, *physica status solidi c* **14**(11), 1700215 (2017).
- [33] A. V. Shevelkov, E. V. Dikarev, R. V. Shpanchenko, and B. A. Popovkin, *Journal of Solid State Chemistry* **114**(2), 379–384 (1995).
- [34] C. Lee, X. Wei, J. W. Kysar, and J. Hone, *Science* **321**(5887), 385–388 (2008).
- [35] A. Bondi, *The Journal of Physical Chemistry* **68**(3), 441–451 (1964).
- [36] R. S. Rowland and R. Taylor, *The Journal of Physical Chemistry* **100**(18), 7384–7391 (1996).
- [37] S. Ryu, A. Schnyder, A. Furusaki, and A. Ludwig, *New Journal of Physics* **12**(6), 065010 (2010).
- [38] J. K. Asbóth, L. Oroszlány, and A. Pályi, *A Short Course on Topological Insulators: Band Structure and Edge States in One and Two Dimensions*, *Lecture Notes in Physics*, Vol. 909 (Springer International Publishing, 2016).
- [39] A. Castellanos-Gomez, R. Roldán, E. Cappelluti, M. Buscema, F. Guinea, H. S. J. van der Zant, and G. A. Steele, *Nano Letters* **13**(11), 5361–5366 (2013).
- [40] Y. Jiang, J. Mao, J. Duan, X. Lai, K. Watanabe, T. Taniguchi, and E. Y. Andrei, *Nano Letters* **17**(5), 2839–2843 (2017).
- [41] J. Martín-Sánchez, R. Trotta, A. Mariscal, R. Serna, G. Piredda, S. Stroj, J. Edlinger, C. Schimpf, J. Aberl, T. Lettner, J. Wildmann, H. Huang, X. Yuan, D. Ziss, J. Stangl, and A. Rastelli, *Semiconductor Science and Technology* **33**(1), 013001 (2017).
- [42] M. Goldsche, J. Sonntag, T. Khodkov, G. J. Verbiest, S. Reichardt, C. Neumann, T. Ouaj, N. von den Driesch, D. Buca, and C. Stampfer, *Nano Letters* **18**(3), 1707–1713 (2018), PMID: 29425440.
- [43] A. K. Kleppe, M. Amboage, and A. P. Jephcoat, *Scientific Reports* **4**, 4989 (2014).
- [44] Z. H. Ni, T. Yu, Y. H. Lu, Y. Y. Wang, Y. P. Feng, and Z. X. Shen, *ACS Nano* **2**(11), 2301–2305 (2008).
- [45] L. F. Braganza and D. L. Worcester, *Biochemistry* **25**(9), 2591–2596 (1986).
- [46] W. L. Vos, L. W. Finger, R. J. Hemley, J. Z. Hu, H. K. Mao, and J. A. Schouten, *Nature* **358**(6381), 46 (1992).
- [47] W. Kullmann, J. Geurts, W. Richter, N. Lehner, H. Rauh, U. Steigenberger, G. Eichhorn, and R. Geick, *physica status solidi (b)* **125**(1), 131–138 (1984).

- [48] Equus: Eötvös Quantum Transport Utilities, <http://eqt.elte.hu/equus/home>.
- [49] J. Ferrer, C. J. Lambert, V. M. García-Suárez, D. Z. Manrique, D. Visontai, L. Oroszlany, R. Rodríguez-Ferradás, I. Grace, S. W. D. Bailey, K. Gillemot, H. Sadeghi, and L. A. Algharagholy, *New Journal of Physics* **16**(9), 093029 (2014).
- [50] C. L. Kane and E. J. Mele, *Phys. Rev. Lett.* **95**(Nov), 226801 (2005).
- [51] R. Winkler, *Spin–Orbit Coupling Effects in Two-Dimensional Electron and Hole Systems*, Springer Tracts in Modern Physics (Springer Berlin Heidelberg, 2003).
- [52] S. H. Lee, H. J. Chung, J. Heo, H. Yang, J. Shin, U. I. Chung, and S. Seo, *ACS Nano* **5**(4), 2964–2969 (2011).
- [53] D. A. Papaconstantopoulos, M. J. Mehl, S. C. Erwin, and M. R. Pederson, *MRS Proceedings* **491**, 221 (1997).
- [54] F. Guinea, *Solid State Communications* **152**(15), 1437–1441 (2012).
- [55] H. Rezaei and A. Phirouznia, *The European Physical Journal B* **91**(11), 295 (2018).
- [56] J. M. Soler, E. Artacho, J. D. Gale, A. García, J. Junquera, P. Ordejón, and Daniel Sánchez-Portal, *Journal of Physics: Condensed Matter* **14**(11), 2745 (2002).
- [57] E. Artacho, E. Anglada, O. Diéguez, J. D. Gale, A. García, J. Junquera, R. M. Martin, P. Ordejón, J. M. Pruneda, D. Sánchez-Portal, and J. M. Soler, *Journal of Physics: Condensed Matter* **20**(6), 064208 (2008).
- [58] J. P. Perdew, K. Burke, and M. Ernzerhof, *Physical Review Letters* **77**(18), 3865–3868 (1996).
- [59] P. Rivero, V. M. García-Suárez, D. Pereñíguez, K. Utt, Y. Yang, L. Bellaiche, K. Park, J. Ferrer, and S. Barraza-Lopez, *Computational Materials Science* **98**, 372–389 (2015).
- [60] H. J. Monkhorst and J. D. Pack, *Physical Review B* **13**(12), 5188–5192 (1976).
- [61] D. D. L. Chung, *Journal of Materials Science* **51**(1), 554–568 (2016).